

Higgs production from anomalous gluon dynamics

Ulrich Haisch^a

^a*Max Planck Institute for Physics,
Boltzmannstr. 8, 85748 Garching, Germany*

E-mail: haisch@mpp.mpg.de

ABSTRACT: We present a two-loop analysis of the contributions to Higgs production via gluon-gluon fusion arising from the triple-gluon operator in the Standard Model effective field theory (SMEFT). Our discussion covers all aspects of renormalization group (RG) improved perturbation theory, including matching and running within the SMEFT. This study can therefore be seen as a blueprint of the intricacies and subtleties that arise in RG improved SMEFT calculations for collider processes beyond the leading order.

Contents

1	Introduction	1
2	Framework	2
3	Calculation	3
4	Beta functions	4
5	Form factor	5
6	RG analysis	7
7	Phenomenology	10
8	Conclusions	12
A	Matching procedure	13
B	HPL formulas	15
C	RG formulas	15

1 Introduction

This year marks the 40th anniversary of the effective Lagrangian for new interactions and flavor conservation [1], which is now known as the Standard Model effective field theory (SMEFT) [2–4]. Since its introduction, the SMEFT has made significant strides and has become a well-established framework for constraining indirect signs of beyond the Standard Model (BSM) physics at the Large Hadron Collider (LHC). This effort places rigorous demands on the theoretical Standard Model (SM) predictions and increasingly also on the precision of the BSM calculations.

While one-loop QCD matching calculations in the SMEFT for LHC processes have seen a degree of automation [5], and the one-loop renormalization group (RG) evolution of the Wilson coefficients for dimension-six SMEFT operators is a solved problem [6–8], two-loop calculations within the SMEFT have only emerged in recent years. Recent progress includes, but is not limited to, the calculations and studies presented in [9–16]. These works share the common feature of achieving two-loop accuracy either in the matching or the running within the SMEFT, but not both. This article seeks to illustrate the full complexity of RG improved perturbation theory beyond the one-loop level in the SMEFT through a nontrivial yet instructive example. The example we consider is the contribution of the

triple-gluon operator to Higgs production in gluon-gluon fusion ($gg \rightarrow h$). Assuming that this operator is the dominant ultraviolet (UV) deformation, the $gg \rightarrow h$ production cross section is modified first at the two-loop level. These corrections stem from three distinct types of contributions, which involve matching and running effects at different perturbative orders. The unphysical dependence on the renormalization scale cancels order by order in perturbation theory only when these corrections are properly combined. By using the relevant SMEFT RG equations (RGEs), one can then resum the large logarithms that appear in the $gg \rightarrow h$ prediction, going beyond leading logarithmic (LL) accuracy.

Another reason for considering the triple-gluon operator contribution to $gg \rightarrow h$ production is that its Wilson coefficient remains relatively weakly constrained by jet observables and top-quark processes [17–22]. In fact, the nominally strongest constraints come from multijet production and rely on the strong enhancement of the quadratic contributions in the Wilson coefficient within the high-energy tails of multijet distributions. This raises questions about the reliability of the effective field theory (EFT) expansion when extracting bounds on the Wilson coefficient of the triple-gluon operator from multijet observables. Given these limitations, indirect precision tests of the triple-gluon operator are of particular interest. In this work, we show that precise LHC measurements of the $gg \rightarrow h$ production cross section can serve as complementary probes of anomalous gluon dynamics.

This article is organized as follows: in Section 2, we present the subset of dimension-six operators relevant to our study. Section 3 provides a brief overview of the key steps in computing the SMEFT corrections to $gg \rightarrow h$. The relevant beta functions are discussed in Section 4, while Section 5 dissects the structure of the SMEFT corrections to the $gg \rightarrow h$ form factor. Section 6 explores the solutions of the RGEs. In Section 7, we analyze the phenomenological implications of our findings. Our conclusions are presented in Section 8. Additional technical details are provided in Appendix A, Appendix B, and Appendix C.

2 Framework

To establish our notation and conventions, we begin by defining the SMEFT Lagrangian:

$$\mathcal{L}_{\text{SMEFT}} = \sum_i C_i(\mu) Q_i. \quad (2.1)$$

Here, $C_i(\mu)$ denotes the dimensionful Wilson coefficients evaluated at the renormalization scale μ , which are associated with the corresponding effective operators Q_i . For the entirety of this article, we assume that all Wilson coefficients are real.

In the Warsaw basis of operators [2], the full set of dimension-six operators relevant to this study includes

$$Q_G = f^{abc} G_\mu^{a,\nu} G_\nu^{b,\rho} G_\rho^{c,\mu}, \quad Q_{tG} = \bar{q} \sigma^{\mu\nu} \tilde{H} T^a t G_{\mu\nu}^a, \quad Q_{HG} = H^\dagger H G_{\mu\nu}^a G^{a,\mu\nu}. \quad (2.2)$$

In this context, $G_{\mu\nu}^a$ is the field strength tensor of $SU(3)_C$, with $T^a = \lambda^a/2$ the generators of the group, where λ^a are the Gell-Mann matrices and f^{abc} are the structure constants. The corresponding gauge coupling will be denoted by g_s . H represents the SM Higgs doublet, and we used $\tilde{H} = \varepsilon \cdot H^*$, where $\varepsilon = i\sigma^2$ is the antisymmetric $SU(2)$ tensor. The

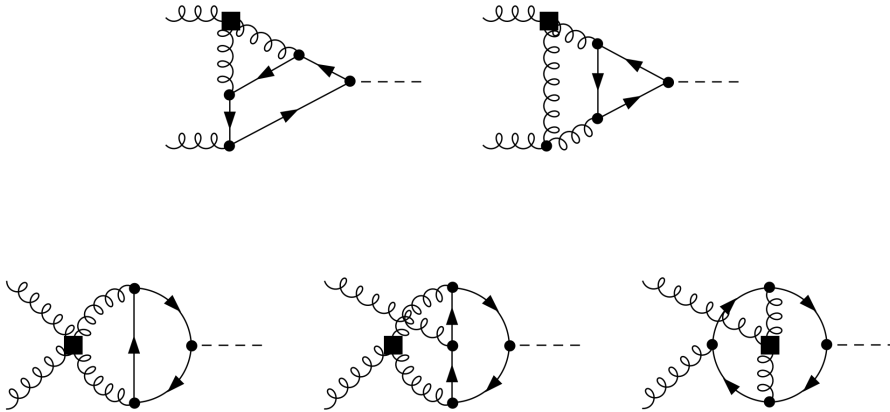


Figure 1. Examples of two-loop contributions to the $gg \rightarrow h$ process involving an insertion of the operator Q_G defined in (2.2). The operator insertions are represented by black boxes, gluons and the Higgs are depicted by wiggly lines and dashed lines, respectively, while the solid lines depict quarks. See the main text for further details.

symbol q represents the left-handed third-generation quark $SU(2)_L$ doublets, while t denotes the right-handed top-quark $SU(2)_L$ singlet. Lastly, notice that for the operator Q_{tG} the sum of the hermitian conjugate is implied in (2.1).

Below, we concentrate on a particular class of BSM scenarios in which, at the high-energy scale Λ , the initial conditions of the Wilson coefficients follow the hierarchy:

$$C_G(\Lambda) \gg C_{tG}(\Lambda) \gg C_{HG}(\Lambda) \simeq 0. \quad (2.3)$$

We remain agnostic about how such scenarios are realized, as the primary goal of this article is to elucidate the rich structure of RG improved perturbation theory in the SMEFT. Indeed, we will see below, obtaining the full leading SMEFT correction to $gg \rightarrow h$ in BSM scenarios of the form (2.3) requires accounting for three types of contributions: (i) two-loop matching contributions involving the tree-level Wilson coefficient C_G , (ii) one-loop matching contributions involving the one-loop evolved Wilson coefficient C_{tG} , and (iii) tree-level matching contributions involving the two-loop evolved Wilson coefficient C_{HG} .

3 Calculation

In our loop calculations, we use dimensional regularization to handle UV singularities in $d = 4 - 2\epsilon$ dimensions, supplemented by the renormalization scale μ and a naive anticommuting γ_5 (NDR) [23]. As traces involving γ_5 do not appear in the calculation, the use of the NDR scheme is evidently consistent. The actual computation was performed using the `Mathematica` packages `FeynRules` [24], `FeynArts` [25], `FormCalc` [26], and `LiteRed` [27]. Specifically, `FeynRules` is used to implement the SMEFT operators (2.2) and generate a `FeynArts` model file. `FeynArts` constructs the relevant Feynman diagrams and amplitudes, while `FormCalc` performs the projection onto form factors (see, e.g., [28]) and handles color

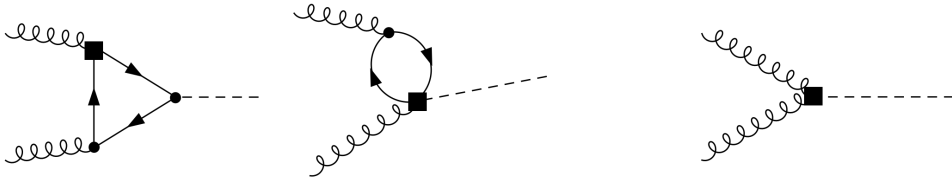


Figure 2. Left: Examples of one-loop diagrams for $gg \rightarrow h$ with a single insertion of Q_{tG} . Right: The tree-level contribution to $gg \rightarrow h$ featuring an insertion of Q_{HG} . The plot styles follow the same conventions as in Figure 1.

and Dirac algebra. Finally, the scalar integrals are reduced to one-loop and two-loop master integrals (MIs) using `LiteRed`. The analytical form of all MIs, except one, is known from the publication [29]. The missing two-loop MI is calculated using differential equation techniques (see, e.g., [30–34]). All MIs can be expressed as Laurent series in ϵ using harmonic polylogarithms (HPLs). As a cross-check, the MIs were numerically evaluated using `AMFlow` [35], and the results agreed with the analytical expressions.

Figure 1 displays representative two-loop Feynman diagrams with a single insertion of the tripe-gluon operator Q_G introduced in (2.2), which contribute to the $gg \rightarrow h$ process. The corresponding unrenormalized amplitude contains both $1/\epsilon^2$ and $1/\epsilon$ poles of UV origin. To achieve a UV-finite result, one must account for the fact that Q_G mixes into the chromomagnetic top-quark dipole operator Q_{tG} at one loop, which in turn mixes into the Higgs-gluon operator Q_{HG} at the same order. All relevant one-loop anomalous dimensions can be found in [7, 8]. After subtracting the appropriate counterterm contributions in the modified minimal subtraction ($\overline{\text{MS}}$) scheme [36], the remaining $1/\epsilon$ pole becomes local (for general discussions of this point see, e.g., [37, 38]). The left-over UV divergence determines the two-loop anomalous dimensions that govern the mixing of Q_G into Q_{HG} . Observe that, numerically, only top-quark loops are important due to the strong Yukawa suppression of all other quarks. Therefore, in the results below, we consider only contributions involving the top-quark Yukawa coupling y_t .

Since the operator Q_G mixes at one-loop and two-loop into Q_{tG} and Q_{HG} , respectively, additional contributions to the $gg \rightarrow h$ process arise from the one-loop and tree-level matrix elements with insertions of these operators. Figure 2 depicts representative graphs. The unrenormalized one-loop amplitude with a Q_{tG} insertion contains a local $1/\epsilon$, which is removed via $\overline{\text{MS}}$ operator renormalization. The corresponding one-loop counterterm can be determined using the SMEFT anomalous dimensions provided in [7, 8]. Finally, the tree-level amplitude with a single insertion of Q_{HG} yields a finite contribution to $gg \rightarrow h$. Further details on the matching calculation can be found in Appendix A.

4 Beta functions

The RG evolution of the Wilson coefficients C_i is dictated by the beta functions:

$$\frac{dC_i}{d \ln \mu} = \beta_i = \sum_{l=1}^{\infty} \frac{\beta_i^{(l)}}{(16\pi^2)^l}. \quad (4.1)$$

The one-loop beta functions $\beta_i^{(1)}$ for the operators in (2.2) relevant to our study are

$$\begin{aligned}\beta_G^{(1)} &= 15g_s^2 C_G, \\ \beta_{tG}^{(1)} &= \left(-\frac{17}{3}g_s^2 + \frac{15}{2}y_t^2\right) C_{tG} + 9g_s^2 y_t C_G - 4g_s y_t C_{HG}, \\ \beta_{HG}^{(1)} &= \left(-14g_s^2 + 6y_t^2\right) C_{HG} - 4g_s y_t C_{tG}.\end{aligned}\tag{4.2}$$

They have been computed in [7, 8]. Note that the coefficients proportional to g_s^2 in the beta functions $\beta_G^{(1)}$ and $\beta_{HG}^{(1)}$ depend on the number of active quark flavors. The given values are based on the assumption of six active quark flavors. Above the dependence of g_s and y_t as well as the Wilson coefficients C_i on the renormalization scale μ has been omitted.

As discussed in the previous section, the local $1/\epsilon$ pole that remains in our two-loop computation of the $gg \rightarrow h$ amplitude can be used to extract the unknown two-loop beta function in the SMEFT¹ that describes the mixing of Q_G into Q_{HG} . We find

$$\beta_{HG}^{(2)} = 207g_s^3 y_t^2 C_G.\tag{4.3}$$

5 Form factor

We now proceed to present the matching corrections to the $gg \rightarrow h$ process involving the Wilson coefficients of the operators (2.2). To establish our notation and normalization, we begin by giving the one-loop contribution to the $gg \rightarrow$ form factor in the SM, induced by the top quark:

$$G^{(1)} = -\frac{6x}{(x-1)^2} + \frac{3x(x+1)^2}{(x-1)^4} H(0, 0; x),\tag{5.1}$$

with

$$x = \frac{\sqrt{1-\tau}-1}{\sqrt{1-\tau}+1}, \quad \tau = \frac{4m_t^2}{m_h^2}.\tag{5.2}$$

Here, $H(0, 0; x)$ is a HPL of weight 2 that represents the ϵ^0 contribution to the massive one-loop triangle integral. The expressions for all HPLs appearing in our calculations in terms of logarithms, dilogarithms, and other well-known functions can be found in Appendix B. Note that the HPL above depends on a single variable, x , known as the Landau variable, which is especially well-suited for describing two-scale Feynman integrals, such as those arising in our work. In the infinite top-quark mass limit, i.e., as $\tau \rightarrow \infty$, one has $x \rightarrow 1$. In this limit, $G^{(1)} \rightarrow 1$, which fixes the normalization of the one-loop SM $gg \rightarrow h$ form factor.

The SMEFT corrections of interest to the $gg \rightarrow h$ form factor can be expressed as the sum of three separate contributions

$$G^{(2)} = \left(\frac{g_s y_t^2}{16\pi^2} F_G C_G + \frac{y_t}{g_s} F_{tG} C_{tG} + \frac{16\pi^2}{g_s^2} F_{HG} C_{HG}\right) v^2,\tag{5.3}$$

where $v = 246.22$ GeV denotes the Higgs vacuum expectation value.

¹Other two-loop anomalous dimensions in the SMEFT have been calculated in [10, 12–14, 39–43].

The function F_G encodes the two-loop corrections originating from Q_G . We obtain

$$\begin{aligned}
F_G(x) = & \frac{1}{x(x+1)^2(x^2-x+1)} \left\{ \frac{72(4x-3)}{(x-1)^2} \right. \\
& + \frac{9}{64} (230x^6 - 2823x^5 - 4228x^4 - 1694x^3 - 3716x^2 - 1799x + 1766) \\
& + \left[\frac{9(1321x^2 - 2516x + 1223)}{2(x-1)^3} \right. \\
& \quad \left. - \frac{9}{16} (26x^6 - 121x^5 - 1464x^4 - 4388x^3 - 7424x^2 - 9103x - 9810) \right] H(0; x) \\
& + \left[\frac{9(696x^3 - 2011x^2 + 1954x - 635)}{2(x-1)^4} \right. \\
& \quad \left. - \frac{9}{4} (6x^6 + 27x^5 - 104x^4 - 563x^3 - 976x^2 - 1175x - 1272) \right] H(0, 0; x) \Big\} \\
& + \frac{1}{x(x^2-x+1)} \left\{ \left[\frac{117}{x-1} - \frac{9}{4} (2x^4 + 41x^3 - 26x^2 - 93x - 54) \right] H(1, 0; x) \right. \\
& \quad \left. - \left[\frac{1026}{x-1} - \frac{27}{4} (2x^4 - 9x^3 - 76x^2 - 143x - 154) \right] H(-1, 0; x) \right\} \\
& - \left[54 + \frac{9x(95x^2 - 194x + 95)}{2(x-1)^4} \right] H(0, 0, 0; x) \tag{5.4} \\
& - \left[126 + \frac{36x(21x^2 - 43x + 21)}{(x-1)^4} \right] H(1, 0, 0; x) + \left[36 - \frac{81x}{(x-1)^2} \right] H(0, 1, 0; x) \\
& + \left[54 + \frac{216x}{(x-1)^2} \right] H(0, 0, 1; x) + \left[72 + \frac{234x}{(x-1)^2} \right] H(0, -1, 0; x) \\
& + \frac{27x}{(x-1)^2} H(x) - 54B(x) - \left\{ \frac{1}{x(x+1)^2(x^2-x+1)} \left[\frac{9(172x-173)}{(x-1)^2} \right. \right. \\
& \quad \left. \left. - \frac{9}{16} (6x^6 - 183x^5 - 660x^4 - 1278x^3 - 1892x^2 - 2547x - 2770) \right] \right. \\
& \quad \left. - \left[18 - \frac{180x}{(x-1)^2} \right] H(0; x) - \frac{27x}{(x-1)^2} H(0, 0; x) - \frac{54x}{(x-1)^2} H(1, 0; x) \right\} H(0, 1; 1) \\
& + \left[252 + \frac{9x(81x^2 - 166x + 81)}{(x-1)^4} \right] H(0, 0, 1; 1) + \frac{135x}{2(x-1)^2} H(0, 0, 0, 1; 1) \\
& - \left[324 - \frac{27(x+1)}{2(x-1)} H(0; x) - \frac{27x}{(x-1)^2} H(0, 0; x) \right] L_t - \frac{27}{2} L_t^2.
\end{aligned}$$

In (5.4), $H(x)$ represents the following specific combination of HPLs of weight 4:

$$\begin{aligned} H(x) &= 3H(1, 0, 0, 0; x) + 2H(0, 1, 0, 0; x) + H(0, 0, 1, 0; x) \\ &\quad + 4H(1, 1, 0, 0; x) + 2H(1, 0, 1, 0; x). \end{aligned} \quad (5.5)$$

Moreover, we have introduced the abbreviations

$$B(x) = 1 - H\left(0; \frac{(1-x)^2}{x} - i\delta\right), \quad L_t = \ln\left(\frac{\mu^2}{m_t^2}\right), \quad (5.6)$$

where $B(x)$ results from the ϵ^0 term in the massless one-loop on-shell bubble integral, with δ being positive and infinitesimally small. Notice that the $i\delta$ prescription is needed here for the correct analytic continuation of $H(0; x)$, which is merely a simple logarithm — see Appendix B.

The function F_{tG} in (5.3) encapsulates the one-loop correction due to the insertion of the operator Q_{tG} . This contribution is explicitly given by:

$$F_{tG} = 3 \left[1 - \frac{x+1}{x-1} H(0; x) - \frac{2x}{(x-1)^2} H(0, 0; x) + 2L_t \right]. \quad (5.7)$$

This result agrees with the findings of [10, 44–46].

The tree-level contribution from Q_{HG} is finally given by

$$F_{HG} = 3. \quad (5.8)$$

Before analyzing the RG flow of the contributions to $gg \rightarrow h$ production arising from the triple-gluon operator, we emphasize that in (5.3), the Wilson coefficients C_G , G_{tG} and C_{HG} , as well as the strong coupling constant g_s and the top-quark Yukawa coupling y_t , are all understood to be evaluated at the renormalization scale μ .

6 RG analysis

We start our study of the RGEs (4.1) by examining the following initial conditions

$$C_G(\Lambda) \neq 0, \quad C_{tG}(\Lambda) = 0, \quad C_{HG}(\Lambda) = 0, \quad (6.1)$$

which corresponds to the extreme case of the hierarchy (2.3), where at the high-energy scale Λ , only the triple-gluon operator is generated through matching to a UV-complete BSM model. Inserting the beta functions (4.2) and (4.3) into the analytical results presented in Appendix C, we obtain the following simple results

$$\begin{aligned} \frac{C_G(\mu)}{C_G(\Lambda)} &\simeq 1 + \frac{g_s^2}{16\pi^2} \left(-\frac{15}{2} L_\Lambda \right), \\ \frac{C_{tG}(\mu)}{C_G(\Lambda)} &\simeq \frac{g_s^2 y_t}{16\pi^2} \left(-\frac{9}{2} L_\Lambda \right), \\ \frac{C_{HG}(\mu)}{C_G(\Lambda)} &\simeq \frac{g_s^3 y_t^2}{256\pi^4} \left(-\frac{9}{2} L_\Lambda^2 - \frac{207}{2} L_\Lambda \right), \end{aligned} \quad (6.2)$$

where

$$L_\Lambda = \ln \left(\frac{\Lambda^2}{\mu^2} \right). \quad (6.3)$$

A few remarks seem warranted. The single logarithm in the evolution of C_G results from the one-loop self-mixing of Q_G . For the running of C_{tG} , the single logarithm arises from the one-loop mixing of Q_G into Q_{tG} . In the case of the evolution of C_{HG} , the double logarithm stems from a two-step mixing process,² namely Q_G mixes into Q_{tG} at one loop, which subsequently mixes into Q_{HG} at the same perturbative order. The single logarithm instead results from the direct two-loop mixing of Q_G into Q_{HG} . Notice that, from the viewpoint of RG improved perturbation theory, the double logarithm in the last line of (6.2) corresponds to a LL effect, while the single logarithm represents a next-to-leading logarithmic (NLL) correction.

Before discussing the resummation of large logarithms, we emphasize the following important point. By inserting the logarithmic expressions for the ratios (6.2) of Wilson coefficients into (5.3), it is a matter of simple algebra to demonstrate that the two-loop SMEFT corrections to the $gg \rightarrow h$ form factor become renormalization scale independent at $\mathcal{O}(g_s y_t^2)$. This occurs because the terms in (5.4) to (5.8) involving L_t terms combine with the L_Λ contributions in (6.2), resulting in logarithms of the form $L = L_t + L_\Lambda = \ln(\Lambda^2/m_t^2)$. The cancellation of renormalization scale dependence provides a strong consistency check for our computation. Indeed, the observation that different types of contributions — incorporating matching and running effects at various perturbative orders — must be included to ensure that observables remain free from unphysical scale dependencies is a general feature of EFTs at the quantum level. The case examined in this article, involving the three operators (2.2) that contribute to $gg \rightarrow h$ production, serves as a nontrivial yet insightful example within the SMEFT framework, highlighting this general aspect of RG improved perturbation theory.

Using the RG formulas presented in Appendix C we can also resum the logarithms appearing in (6.2). We obtain

$$\begin{aligned} \frac{C_G(\mu)}{C_G(\Lambda)} &\simeq \left(\frac{\alpha_s(\mu)}{\alpha_s(\Lambda)} \right)^{-\frac{15}{14}}, \\ \frac{C_{tG}(\mu)}{C_G(\Lambda)} &\simeq -\frac{9g_s^2(\Lambda)y_t(\Lambda)}{16\pi^2} \left[\frac{14011}{935} (\alpha_s(\mu))^{\frac{3}{50}} - \frac{10789}{4554} (\alpha_s(\mu))^{-\frac{938}{1327}} \right], \\ \frac{C_{HG}(\mu)}{C_G(\Lambda)} &\simeq -\frac{9g_s^3(\Lambda)y_t^2(\Lambda)}{128\pi^4} \left[\frac{69439}{77} (\alpha_s(\mu))^{\frac{21}{29}} + \frac{1803}{83} (\alpha_s(\mu))^{-\frac{187}{222}} - \frac{9421}{35} (\alpha_s(\mu))^{-\frac{4}{53}} \right] \\ &\quad - \frac{207g_s^3(\Lambda)y_t^2(\Lambda)}{256\pi^4} \left[\frac{98329}{981} (\alpha_s(\mu))^{\frac{470}{649}} - \frac{12317}{480} (\alpha_s(\mu))^{\frac{138}{875}} \right]. \end{aligned} \quad (6.4)$$

Here, $\alpha_s = g_s^2/(4\pi)$, and the results for the second and third ratios of Wilson coefficients use $g_s(\Lambda) \simeq 1.065$ and $y_t(\Lambda) \simeq 0.854$, valid for $\Lambda = 2 \text{ TeV}$. The numerical values quoted

²The importance of logarithmic corrections resulting from a chain of operator mixings has been emphasized in several previous studies, including [47–60].

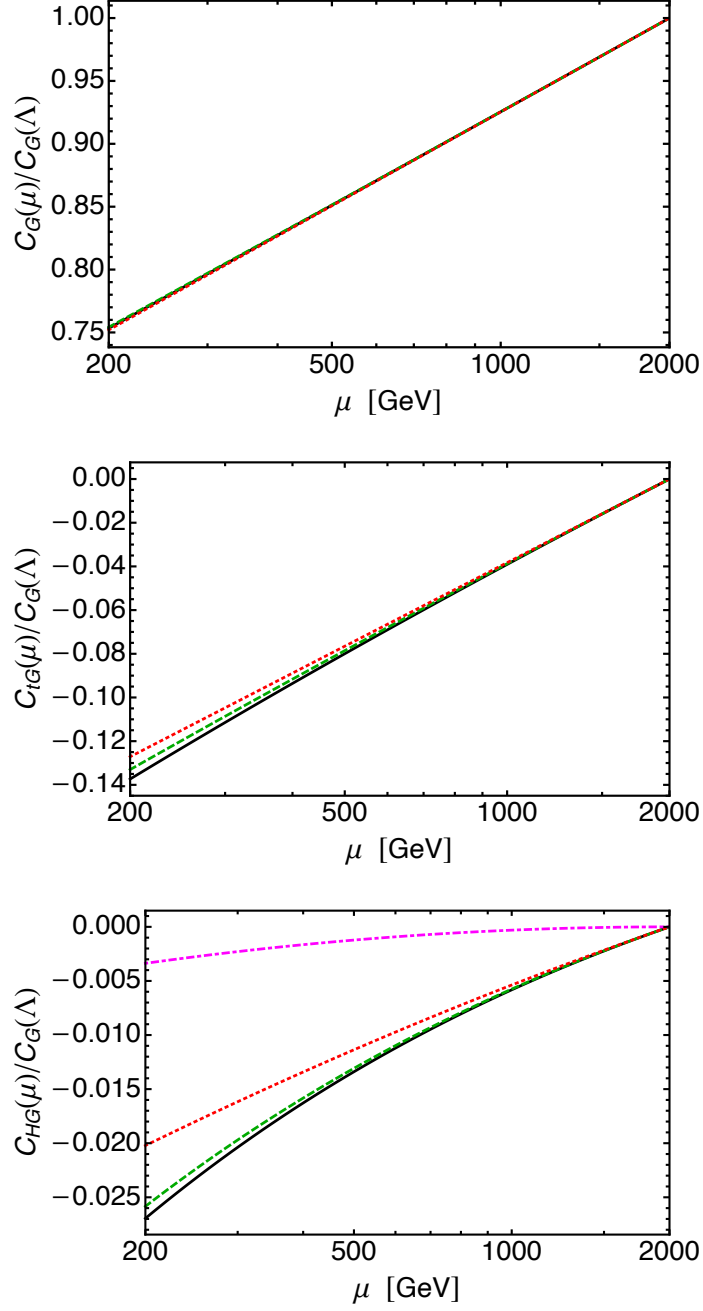


Figure 3. Ratios $C_G(\mu)/C_G(\Lambda)$ (top), $C_{tG}(\mu)/C_G(\Lambda)$ (middle), and $C_{HG}(\mu)/C_G(\Lambda)$ (bottom) plotted as functions of the renormalization scale μ . At the high-energy scale $\Lambda = 2$ TeV, only the Wilson coefficient $C_G(\Lambda)$ is assumed to be nonzero. In the plots, the solid black curve depicts the numerical solution computed using `DsixTools 2.0`, while the green dashed curve and red dotted curve represent the resummed analytic results and the logarithmically accurate results, respectively. The magenta dash-dotted curve in the bottom panel finally represents the LL-accurate result of the ratio $C_{HG}(\mu)/C_G(\Lambda)$. Consult the main text for additional explanations.

were obtained using `DsixTools` 2.0 [61]. Note that the double-logarithmic contribution, representing an LL term in the running of C_{HG} , arises from the first line of the third expression in (6.4), whereas the single-logarithmic correction, corresponding to an NLL term, originates from the second line.

In Figure 3, we present a comparison between the numerical solutions for the ratios $C_G(\mu)/C_G(\Lambda)$, $C_{tG}(\mu)/C_G(\Lambda)$, and $C_{HG}(\mu)/C_G(\Lambda)$ of Wilson coefficients and their corresponding approximations in (6.2) and (6.4). The numerical solutions, shown as solid black curves, are obtained using `DsixTools` 2.0 through direct numerical integration of the RGEs. The version of `DsixTools` 2.0 used has been modified to include the two-loop beta function $\beta_{HG}^{(2)}$ from (4.3). The green dashed curves depict the resummed analytic results, while the red dotted curves represent the logarithmically accurate results. In the case of $C_{HG}(\mu)/C_G(\Lambda)$, the LL-accurate result is finally shown as a magenta dash-dotted curve. We further note that the resummed analytic results presented were obtained using the LO QCD approximation for the running strong coupling constant, as given in (C.2). This choice is justified by the fact that the LO QCD running of $\alpha_s(\mu)$ was used in deriving the approximations in (6.4).

The first notable observation from Figure 3 is that the expressions in (6.4) provide accurate approximations to the exact numerical results across all three cases studied. The small discrepancies observed can be attributed to the inclusion of higher-order corrections in the evolution of g_s and y_t within `DsixTools` 2.0, which are not accounted for in our approximations. We note that using the `DsixTools` 2.0 prediction for $\alpha_s(\mu)$ would result in an almost perfect agreement between the resummed analytic results and the exact numerical results. In the case of $C_G(\mu)/C_G(\Lambda)$ and $C_{tG}(\mu)/C_G(\Lambda)$, we find that the resummation of logarithmic effects through the RGEs has only a minor numerical impact. However, for $C_{HG}(\mu)/C_G(\Lambda)$, resummation plays a more significant role. Consequently, the ratio given in (6.2), which includes both double-logarithmic and single-logarithmic terms, is a less accurate approximation. This is due to the large numerical coefficient in the two-loop beta function (4.3). Therefore, the LL-accurate result for $C_{HG}(\mu)/C_G(\Lambda)$ is also not a good approximation. The findings above show that the dominant RG effects arise from operator mixings proportional to powers of g_s or y_t , as well as the evolution of these parameters under the RG flow. As discussed in this section and in Appendix C, corrections of this nature can be resummed, resulting in relatively compact analytic expressions.

7 Phenomenology

Utilizing the form factors given in (5.1) and (5.3), the Higgs production cross section in the $gg \rightarrow h$ process, incorporating the effects of the SMEFT operators introduced in (2.2), can be expressed as

$$\sigma(gg \rightarrow h) = \frac{\alpha_s^2}{576\pi} \frac{1}{v^2} |G^{(1)} + G^{(2)}|^2. \quad (7.1)$$

To linear order in the Wilson coefficients, the resulting modification of the signal strength relative to the SM is therefore given by

$$\delta\kappa_g = \frac{2\text{Re}(G^{(1)}G^{(2)*})}{|G^{(1)}|^2}. \quad (7.2)$$

As a concrete example, let us derive the current constraint on the high-scale Wilson coefficients of Q_G using the existing LHC signal strength measurements for Higgs production in the $gg \rightarrow h$ channel. Taking $m_t = 162.5 \text{ GeV}$ and $m_h = 125.2 \text{ GeV}$ from the Particle Data Group [62] as input parameters, and setting $\Lambda = 2 \text{ TeV}$, we obtain the following numerical result

$$\frac{\delta\kappa_g}{v^2} = 1.87 \left[1 - 0.45 \ln\left(\frac{\mu^2}{m_h^2}\right) + 0.06 \ln^2\left(\frac{\mu^2}{m_h^2}\right) \right] C_G(\Lambda), \quad (7.3)$$

for the modification of the $gg \rightarrow h$ signal strength in the BSM scenario (6.4). The numerical values of the low-scale Wilson coefficients entering (7.3) have been obtained using `DsixTools 2.0`. Regarding the above result, it is important to stress that the sensitivity of $\delta\kappa_g$ to $C_G(\Lambda)$ is reduced due to a strong destructive interference between the contributions to (6.4) from the form factors F_G and F_{HG} . This cancellation, however, is not coincidental but stems from the renormalization scale independence of $G^{(2)}$ up to NLL accuracy.

At the 68% confidence level (CL), the ATLAS collaboration presents the following constraint on the signal strength of Higgs production in $gg \rightarrow h$:

$$\kappa_g = 0.949_{-0.067}^{+0.072}. \quad (7.4)$$

This limit is based on the full LHC Run II dataset [63]. By applying (7.3) with $\mu = m_h$, we derive the following bound

$$C_G(\Lambda) = \frac{[-1.04, 0.19]}{\text{TeV}^2}, \quad (7.5)$$

based on (7.4). Limits on the Wilson coefficient C_G have also been obtained in [17–22]. The nominal best bound, $|C_G| < 0.031 \text{ TeV}^{-2}$ at 95% CL, was derived in [20] using LHC dijet angular distributions. Although the constraint given in (7.5) is weaker than the latter limit, it is important to consider the following points. The constraints on the triple-gluon operator from multijet production are driven by terms proportional to $|C_G|^2$, while the linear contributions remain negligible, even when the number of jets exceeds two [18, 19]. This feature arises from the strong energy enhancement of the quadratic SMEFT corrections compared to the SM background. In contrast, the limit (7.5) emerges at linear order and depends only on virtualities well below Λ . From the standpoint of the robustness and validity of the EFT expansion, the bound on C_G derived here is thus more reliable than the limits obtained from multijet production. Consequently, we believe that LHC measurements of the $gg \rightarrow h$ production cross section can act as complementary probes of anomalous gluon dynamics.

8 Conclusions

This article is part of the SMEFT precision program (see, e.g., [9–16, 39–42, 45]), which aims on improving the precision of these calculations beyond the one-loop level. Specifically, we performed a comprehensive two-loop analysis of the contributions to Higgs production via $gg \rightarrow h$ from the triple-gluon operator, which captures anomalous gluon dynamics. Working in the broken phase of the theory, we determined the exact dependence of the relevant amplitudes on the Higgs and top-quark masses. We also provided a concise discussion of the renormalization procedure that guarantees the UV finiteness of the resulting two-loop $gg \rightarrow h$ form factor. Additional details regarding the matching procedure at one and two loops can be found in Appendix A. It turns out that the renormalization of the calculated two-loop amplitudes requires an unknown two-loop SMEFT anomalous dimension, which we computed as a byproduct.

By analyzing the RG flow of the relevant SMEFT Wilson coefficients, we have demonstrated that achieving a renormalization scale independent result for the $gg \rightarrow h$ production cross section at next-to-leading order in the SMEFT, in the case under study, requires accounting for three types of contributions: (i) two-loop matching contributions involving the triple-gluon operator, (ii) one-loop matching contributions associated to the chromomagnetic top-quark dipole operator, and (iii) tree-level matching contributions arising from insertions of the Higgs-gluon operator. We emphasized that the necessity of including distinct types of contributions, involving matching and running effects at different perturbative orders, to achieve renormalization scale independent results is a general feature of SMEFT calculations beyond the tree level. The case studied in this article provides a nontrivial yet instructive two-loop example that emphasizes this general aspect of RG improved perturbation theory.

Utilizing the SMEFT RGEs, we then resummed the large logarithms that appear in the $gg \rightarrow h$ prediction. Specifically, we derived simple analytic expressions and compared them with the exact results obtained from `DsixTools 2.0` [61] via direct numerical integration of the RGEs. The presented expressions provide accurate approximations to the exact numerical results in all three cases analyzed. We found that resumming logarithmic effects has a limited numerical impact on our results. The only partial exception is the Wilson coefficient of the Higgs-gluon operator, which receives sizeable NLL corrections due to the newly calculated two-loop beta function. Our findings demonstrate that, in typical phenomenological applications, the dominant SMEFT RG effects stem from operator mixings that scale with powers of the strong coupling constant or the top-quark Yukawa coupling, along with the RG evolution of these parameters. A general framework for resumming SMEFT corrections of this type is outlined in Appendix C. Our approach is based on the pedagogical discussion provided in [51].

We also explored the phenomenological implications of our two-loop calculation. To this end, we derived a numerical expression for the modification of the signal strength in the $gg \rightarrow h$ process. The derived formula was subsequently used to obtain constraints on the high-scale Wilson coefficient of the triple-gluon operator. We found that the resulting bound is weaker than the existing constraints from multijet production [18–20]. However, when

comparing these constraints, it is important to remember that the latter bounds stem from the strong enhancement of the quadratic contributions in the Wilson coefficient within the high-energy tails of multijet distributions, while the $gg \rightarrow h$ process probes the linear corrections at virtualities well below the UV cut-off. From the perspective of the robustness and validity of the EFT expansion, the limit derived here is therefore more reliable than those obtained from multijet production. Given this complementarity, we believe that constraints on the triple-gluon operator from $gg \rightarrow h$ should be included in global SMEFT analyses. The compact analytical and numerical expressions presented in this study should prove useful in this context.

Acknowledgments

UH expresses gratitude to Marco Niggetiedt, Luc Schnell, and Ben Stefanek for their collaborations on related subjects. He would also like to thank Gino Isidori and Zach Polonsky for inviting him to “ZPW2025: Particle Physics from Low to High Energies”. A part of this workshop was dedicated to celebrating Daniel Wyler’s 75th birthday, recognizing him as one of the two pioneers of the SMEFT [1], among other accomplishments. Happy birthday, Daniel! This work has benefited greatly from the workshop’s relaxed atmosphere and the long train ride between Munich and Zurich, and back again. The Feynman diagrams in this article were created using `FeynArts` [25].

A Matching procedure

In this appendix, we provide a more detailed explanation of the matching procedure that yields the results (5.4) and (5.7). We start by discussing the one-loop matching that leads to the term F_{tG} in the two-loop form factor $G^{(2)}$ as presented in (5.3). In this case, the relevant matching equation reads:

$$K^{(1)} = A^{(1)} - \frac{Z_{tG,HG}^{(1),1}}{\epsilon}. \quad (\text{A.1})$$

Here, $A^{(1)}$ denotes the bare one-loop amplitude resulting from single insertions of Q_{tG} , normalized to the tree-level $gg \rightarrow h$ matrix element of Q_{HG} , with an overall loop factor of $(16\pi^2)^{-1}$ factored out. This amplitude arises from the Feynman diagrams shown on the left-hand side of Figure 2. The symbol $Z_{tG,HG}^{(1),1}$ represents the one-loop $1/\epsilon$ pole of the Z factor, which accounts for the mixing of Q_{tG} into Q_{HG} . Specifically, it is given by

$$Z_{tG,HG}^{(1),1} = 2g_s y_t. \quad (\text{A.2})$$

Observe that this Z factor determines the coefficient of C_{tG} in the one-loop beta function $\beta_{HG}^{(1)}$ given in (4.2). By evaluating the bare one-loop amplitude $A^{(1)}$ up to order ϵ in the Laurent series and carrying out the matching, we obtain:

$$K^{(1)} = g_s y_t \left(K_0^{(1)} + \epsilon K_\epsilon^{(1)} \right), \quad (\text{A.3})$$

where

$$\begin{aligned}
K_0^{(1)} &= 1 - \frac{x+1}{x-1} H(0; x) - \frac{2x}{(x-1)^2} H(0, 0; x) + 2L_t, \\
K_\epsilon^{(1)} &= 1 - \frac{x+1}{x-1} H(0; x) - \frac{x^2 - 2x - 1}{(x-1)^2} H(0, 0; x) + \frac{2(x+1)}{x-1} H(-1, 0; x) \\
&\quad - \frac{2x}{(x-1)^2} H(0, 0, 0; x) + \frac{4x}{(x-1)^2} H(0, -1, 0; x) \\
&\quad + \left[\frac{2x}{x-1} + \frac{2x}{(x-1)^2} H(0; x) \right] H(0, 1; 1) + \frac{6x}{(x-1)^2} H(0, 0, 1; 1) \\
&\quad + \left[1 - \frac{x+1}{x-1} H(0; x) - \frac{2x}{(x-1)^2} H(0, 0; x) \right] L_t + L_t^2.
\end{aligned} \tag{A.4}$$

Notice that $K_0^{(1)}$ matches the result in (5.7) apart from an overall factor of 3, which cancels out when considering that the tree-level $gg \rightarrow h$ matrix element of Q_{HG} , in the normalization of (5.3), is also 3. See (5.8).

The matching equation required to determine the term F_G in the two-loop form factor $G^{(2)}$ from (5.3) is given by:

$$K^{(2)} = A^{(2)} - \left(\frac{Z_{G,HG}^{(2),2}}{\epsilon^2} + \frac{Z_{G,HG}^{(2),1}}{\epsilon} \right) - \frac{Z_{G,tG}^{(1),1}}{\epsilon} K^{(1)}. \tag{A.5}$$

The symbol $A^{(2)}$ represents the bare two-loop amplitude with a Q_G insertion, normalized to the tree-level $gg \rightarrow h$ matrix element of Q_{HG} , with $(16\pi^2)^{-2}$ factored out. It arises from the graphs displayed in Figure 1. The two-loop Z factors in (A.5) are given by

$$Z_{G,HG}^{(2),2} = \frac{Z_{G,tG}^{(1),1} Z_{tG,HG}^{(1),1}}{2}, \quad Z_{G,HG}^{(2),1} = -\frac{207}{4} g_s^3 y_t^2. \tag{A.6}$$

Notably, the two-loop $1/\epsilon^2$ pole can be expressed as a product of one-loop $1/\epsilon$ poles, reflecting the locality of UV divergences (see, e.g., [37, 38]). The two-loop $1/\epsilon$ pole, on the other hand, is related to the new beta function $\beta_{HG}^{(2)}$ in (4.3). The value of the Z factor $Z_{tG,HG}^{(1),1}$ is given in (A.2), while the one-loop $1/\epsilon$ pole of the Z factor describing the mixing of Q_G into Q_{tG} reads:

$$Z_{G,tG}^{(1),1} = -\frac{9}{2} g_s^2 y_t. \tag{A.7}$$

This Z factor is related to the coefficient of C_G in the one-loop beta function $\beta_C^{(1)}$ from (4.2). Notice that in (A.5), the order ϵ term of $K^{(1)}$, namely $K_\epsilon^{(1)}$, yields a finite contribution when multiplied with the $1/\epsilon$ factor proportional to $Z_{G,tG}^{(1),1}$. By combining the bare two-loop amplitude $A^{(2)}$ with the counterterms specified in (A.5), all UV poles cancel, yielding a finite expression for $K^{(2)}$. Up to an overall normalization factor, this result matches the expression for F_G as given in (5.4).

B HPL formulas

The HPLs in this article can all be rewritten in terms of logarithms, dilogarithms, and similar functions using the HPL package [64]. To make our paper self-contained, we provide all relevant formulas below.

The HPLs up to weight 3 that feature in our calculations are given by:

$$\begin{aligned}
H(0; x) &= \ln(x) , \\
H(0, 0; x) &= \frac{1}{2} \ln^2(x) , \\
H(1, 0; x) &= -\ln(x) \ln(1-x) - \text{Li}_2(x) , \\
H(-1, 0; x) &= \ln(x) \ln(1+x) + \text{Li}_2(-x) , \\
H(0, 0, 0; x) &= \frac{1}{6} \ln^3(x) , \\
H(1, 0, 0; x) &= -\frac{1}{2} \ln(1-x) \ln^2(x) - \ln(x) \text{Li}_2(x) + \text{Li}_3(x) , \\
H(0, 1, 0; x) &= \ln(x) \text{Li}_2(x) - 2\text{Li}_3(x) , \\
H(0, 0, 1; x) &= \text{Li}_3(x) , \\
H(0, -1, 0; x) &= -\ln(x) \text{Li}_2(-x) + 2\text{Li}_3(-x) .
\end{aligned} \tag{B.1}$$

Here, $\text{Li}_2(x)$ and $\text{Li}_3(x)$ represent the dilogarithm and trilogarithm, respectively.

HPLs of weight 4 appear in (5.4) only in the specific combination (5.5). Expressed through commonly known functions, we find

$$\begin{aligned}
H(x) &= \ln^2(x) \ln^2(1-x) - \frac{1}{2} \ln^3(x) \ln(1-x) + 2 \ln(x) \ln(1-x) \text{Li}_2(x) \\
&\quad - \frac{1}{2} \ln^2(x) \text{Li}_2(x) + [\text{Li}_2(x)]^2 .
\end{aligned} \tag{B.2}$$

The HPLs with argument 1 required in this article are

$$H(0, 1; 1) = \frac{\pi^2}{6} , \quad H(0, 0, 1; 1) = \zeta(3) , \quad H(0, 0, 0, 1; 1) = \frac{\pi^4}{90} , \tag{B.3}$$

with $\zeta(3) \simeq 1.20206$, the value of the Riemann zeta function at argument 3.

C RG formulas

In this appendix, we present approximate analytical solutions for the coupled RGEs discussed in our article. Our approach follows, to some extent, the discussion in [51].

To derive approximate analytical solutions to (4.1), we begin by considering the RGE for the strong coupling constant $\alpha_s(\mu)$. At leading order (LO) in QCD, it is given by

$$\frac{d\alpha_s}{d \ln \mu} = -\beta_0 \frac{\alpha_s^2}{2\pi^2} , \quad \beta_0 = 11 - \frac{2}{3} N_F , \tag{C.1}$$

where β_0 denotes the LO coefficient of the QCD beta function, while N_F represents the number of active quark flavors at the renormalization scale μ . The solution to (C.1) reads

$$\alpha_s(\mu) \simeq \frac{\alpha_s(\mu_0)}{1 - \frac{\alpha_s(\mu_0)}{4\pi} \beta_0 \ln\left(\frac{\mu_0^2}{\mu^2}\right)}. \quad (\text{C.2})$$

The beta functions in (4.2) and (4.3) depend not only on α_s but also on y_t . The logarithms associated to the running of the top-quark Yukawa coupling can be resummed by using the following RGE [65, 66]:

$$\frac{dy_t}{d \ln \mu} = -\frac{y_t}{16\pi^2} \left(4\pi\gamma_m^0 \alpha_s - \frac{9}{2} y_t^2 \right), \quad \gamma_m^0 = 8. \quad (\text{C.3})$$

Here, γ_m^0 denotes the LO anomalous dimension of the quark mass in QCD. On the right-hand side of the differential equation, we have included the numerically dominant corrections proportional to α_s and y_t^2 . By utilizing (C.1) as well as the approximate scale independence of $y_t^2(\mu)/\alpha_s(\mu) = \text{const.}$ [51, 67, 68], we obtain the following solution

$$\frac{y_t(\mu)}{y_t(\mu_0)} \simeq \eta^{\frac{y}{b}}, \quad (\text{C.4})$$

with

$$\eta = \frac{\alpha_s(\mu)}{\alpha_s(\mu_0)}, \quad b = 8\pi\beta_0, \quad y = 4\pi\gamma_m^0 \left(1 - \frac{9}{8\pi\gamma_m^0} \frac{y_t^2(\mu_0)}{\alpha_s(\mu_0)} \right). \quad (\text{C.5})$$

The first type of operator mixing relevant to our analysis is the self-mixing of an operator Q_i . Solving the corresponding RGE at the one-loop order yields

$$\frac{C_i(\mu)}{C_i(\mu_0)} \simeq \eta^{-\frac{g_i}{b}} \simeq 1 - \frac{1}{16\pi^2} \frac{\gamma_i(\mu_0)}{2} \ln\left(\frac{\mu_0^2}{\mu^2}\right), \quad (\text{C.6})$$

where we introduced

$$g_i = \frac{\gamma_i(\mu_0)}{\alpha_s(\mu_0)}, \quad (\text{C.7})$$

with $\gamma_i(\mu_0)$ the scale-independent anomalous dimension describing the self-mixing of Q_i . Observe that in the final expression of (C.6), we have expanded the resummed result, retaining only the LL term. From (C.6), one can directly obtain the first line of (6.4).

The second type of RG evolution we consider involves the mixing of an operator Q_i into Q_j , with both operators potentially having nonzero self-mixing. Assuming $C_j(\mu_0) = 0$ and that the anomalous dimension γ_{ji} , which governs this mixing, receives a one-loop contribution proportional to $g_s^2 y_t$, we obtain

$$\frac{C_j(\mu)}{C_i(\mu_0)} \simeq -\frac{\gamma_{ji}(\mu_0)}{\alpha_s(\mu)} \frac{1}{y - g_i + g_j} \left(\eta^{\frac{b+y-g_i}{b}} - \eta^{\frac{b-g_j}{b}} \right) \simeq -\frac{1}{16\pi^2} \frac{\gamma_{ji}(\mu_0)}{2} \ln\left(\frac{\mu_0^2}{\mu^2}\right), \quad (\text{C.8})$$

where the symbols b , y , and g_i are defined in (C.5) and (C.7), respectively. We emphasize that in the first expression of (C.8), the logarithms associated with the factors g_s and y_t that appear in all the anomalous dimensions are resummed. The final result, on the other hand, retains only the LL term, which is proportional to the scale-independent anomalous

dimension $\gamma_{ji}(\mu_0)$ that describes the mixing of Q_i into Q_j . Notice that (C.8) allows for a direct derivation of the second line in (6.4).

The third type of RG corrections we aim to resum involves two-step mixing processes. Here, the running occurs through the one-loop mixing of the operator Q_i into an intermediate operator Q_m , which then undergoes one-loop mixing into Q_j . Assuming $C_j(\mu_0) = C_m(\mu_0) = 0$, and that γ_{mi} and γ_{jm} receive one-loop contributions proportional to $g_s^2 y_t$ and $g_s y_t$, respectively, while $\gamma_{ji} = 0$ at this order, we find

$$\begin{aligned} \frac{C_j(\mu)}{C_i(\mu_0)} &\simeq -\frac{\gamma_{jm}(\mu_0)\gamma_{mi}(\mu_0)}{\alpha_s^2(\mu)} \left[\frac{2}{y-g_i+g_m} \left(\frac{\eta^{\frac{3b+4y-2g_i}{2b}}}{b-4y+2g_i-2g_j} - \frac{\eta^{\frac{3b+2y-2g_m}{2b}}}{b-2y-2g_j+2g_m} \right) \right. \\ &\quad \left. - \frac{4\eta^{\frac{2b-g_j}{b}}}{(b-4y+2g_i-2g_j)(b-2y-2g_j+2g_m)} \right] \quad (\text{C.9}) \\ &\simeq \frac{1}{512\pi^4} \frac{\gamma_{jm}(\mu_0)\gamma_{mi}(\mu_0)}{4} \ln^2 \left(\frac{\mu_0^2}{\mu^2} \right). \end{aligned}$$

The expressions for b , y , and g_i are provided in (C.5) and (C.7). The first expression in (C.9) represents the resummed result, while the final expression corresponds to the LL term, which is proportional to the product $\gamma_{jm}(\mu_0)\gamma_{mi}(\mu_0)$ of scale-independent anomalous dimensions. Notably, (C.9) in combination with (C.8) allows for deriving the final expression in (6.4).

References

- [1] W. Buchmüller and D. Wyler, *Nucl. Phys. B* **268**, 621 (1986).
- [2] B. Grzadkowski, M. Iskrzynski, M. Misiak, and J. Rosiek, *JHEP* **10**, 085 (2010), [arXiv:1008.4884 \[hep-ph\]](#).
- [3] I. Brivio and M. Trott, *Phys. Rept.* **793**, 1 (2019), [arXiv:1706.08945 \[hep-ph\]](#).
- [4] G. Isidori, F. Wilsch, and D. Wyler, *Rev. Mod. Phys.* **96**, 015006 (2024), [arXiv:2303.16922 \[hep-ph\]](#).
- [5] C. Degrande, G. Durieux, F. Maltoni, K. Mimasu, E. Vryonidou, and C. Zhang, *Phys. Rev. D* **103**, 096024 (2021), [arXiv:2008.11743 \[hep-ph\]](#).
- [6] E. E. Jenkins, A. V. Manohar, and M. Trott, *JHEP* **10**, 087 (2013), [arXiv:1308.2627 \[hep-ph\]](#).
- [7] E. E. Jenkins, A. V. Manohar, and M. Trott, *JHEP* **01**, 035 (2014), [arXiv:1310.4838 \[hep-ph\]](#).
- [8] R. Alonso, E. E. Jenkins, A. V. Manohar, and M. Trott, *JHEP* **04**, 159 (2014), [arXiv:1312.2014 \[hep-ph\]](#).
- [9] U. Haisch, D. J. Scott, M. Wiesemann, G. Zanderighi, and S. Zanoli, *JHEP* **07**, 054 (2022), [arXiv:2204.00663 \[hep-ph\]](#).
- [10] S. Di Noi, R. Gröber, G. Heinrich, J. Lang, and M. Vitti, *Phys. Rev. D* **109**, 095024 (2024), [arXiv:2310.18221 \[hep-ph\]](#).

- [11] R. Gauld, U. Haisch, and L. Schnell, *JHEP* **01**, 192 (2024), [arXiv:2311.06107 \[hep-ph\]](#).
- [12] G. Heinrich and J. Lang, *JHEP* **05**, 121 (2024), [arXiv:2311.15004 \[hep-ph\]](#).
- [13] S. Di Noi, R. Gröber, and M. K. Mandal, *JHEP* **12**, 220 (2025), [arXiv:2408.03252 \[hep-ph\]](#).
- [14] L. Born, J. Fuentes-Martín, S. Kvedaraitė, and A. E. Thomsen, (2024), [arXiv:2410.07320 \[hep-ph\]](#).
- [15] U. Haisch and L. Schnell, *JHEP* **02**, 038 (2025), [arXiv:2410.13304 \[hep-ph\]](#).
- [16] M. Bonetti, R. V. Harlander, D. Korneev, M.-M. Long, K. Melnikov, R. Röntsch, and D. M. Tagliabue, (2025), [arXiv:2502.12846 \[hep-ph\]](#).
- [17] D. Ghosh and M. Wiebusch, *Phys. Rev. D* **91**, 031701 (2015), [arXiv:1411.2029 \[hep-ph\]](#).
- [18] F. Krauss, S. Kuttimalai, and T. Plehn, *Phys. Rev. D* **95**, 035024 (2017), [arXiv:1611.00767 \[hep-ph\]](#).
- [19] V. Hirschi, F. Maltoni, I. Tsirikos, and E. Vryonidou, *JHEP* **07**, 093 (2018), [arXiv:1806.04696 \[hep-ph\]](#).
- [20] R. Goldouzian and M. D. Hildreth, *Phys. Lett. B* **811**, 135889 (2020), [arXiv:2001.02736 \[hep-ph\]](#).
- [21] D. Bardhan, D. Ghosh, P. Jain, and A. M. Thalappilil, *Phys. Rev. D* **103**, 115003 (2021), [arXiv:2010.13402 \[hep-ph\]](#).
- [22] J. Ellis, M. Madigan, K. Mimasu, V. Sanz, and T. You, *JHEP* **04**, 279 (2021), [arXiv:2012.02779 \[hep-ph\]](#).
- [23] M. S. Chanowitz, M. Furman, and I. Hinchliffe, *Nucl. Phys. B* **159**, 225 (1979).
- [24] A. Alloul, N. D. Christensen, C. Degrande, C. Duhr, and B. Fuks, *Comput. Phys. Commun.* **185**, 2250 (2014), [arXiv:1310.1921 \[hep-ph\]](#).
- [25] T. Hahn, *Comput. Phys. Commun.* **140**, 418 (2001), [arXiv:hep-ph/0012260](#).
- [26] T. Hahn, S. Paßehr, and C. Schappacher, *PoS LL2016*, 068 (2016), [arXiv:1604.04611 \[hep-ph\]](#).
- [27] R. N. Lee, *J. Phys. Conf. Ser.* **523**, 012059 (2014), [arXiv:1310.1145 \[hep-ph\]](#).
- [28] M. Steinhauser, *Phys. Rept.* **364**, 247 (2002), [arXiv:hep-ph/0201075](#).
- [29] C. Anastasiou, S. Beerli, S. Bucherer, A. Daleo, and Z. Kunszt, *JHEP* **01**, 082 (2007), [arXiv:hep-ph/0611236](#).
- [30] A. V. Kotikov, *Phys. Lett. B* **254**, 158 (1991).
- [31] E. Remiddi, *Nuovo Cim. A* **110**, 1435 (1997), [arXiv:hep-th/9711188](#).
- [32] T. Gehrmann and E. Remiddi, *Nucl. Phys. B* **580**, 485 (2000), [arXiv:hep-ph/9912329](#).
- [33] M. Argeri and P. Mastrolia, *Int. J. Mod. Phys. A* **22**, 4375 (2007), [arXiv:0707.4037 \[hep-ph\]](#).
- [34] J. M. Henn, *J. Phys. A* **48**, 153001 (2015), [arXiv:1412.2296 \[hep-ph\]](#).
- [35] X. Liu and Y.-Q. Ma, *Comput. Phys. Commun.* **283**, 108565 (2023), [arXiv:2201.11669 \[hep-ph\]](#).
- [36] W. A. Bardeen, A. J. Buras, D. W. Duke, and T. Muta, *Phys. Rev. D* **18**, 3998 (1978).
- [37] K. G. Chetyrkin, M. Misiak, and M. Münz, *Nucl. Phys. B* **518**, 473 (1998), [arXiv:hep-ph/9711266](#).

- [38] P. Gambino, M. Gorbahn, and U. Haisch, *Nucl. Phys. B* **673**, 238 (2003), [arXiv:hep-ph/0306079](#).
- [39] M. Gorbahn and U. Haisch, *JHEP* **10**, 094 (2016), [arXiv:1607.03773 \[hep-ph\]](#).
- [40] Z. Bern, J. Parra-Martinez, and E. Sawyer, *JHEP* **10**, 211 (2020), [arXiv:2005.12917 \[hep-ph\]](#).
- [41] Q. Jin, K. Ren, and G. Yang, *JHEP* **04**, 180 (2021), [arXiv:2011.02494 \[hep-ph\]](#).
- [42] E. E. Jenkins, A. V. Manohar, L. Naterop, and J. Pagès, *JHEP* **02**, 131 (2024), [arXiv:2310.19883 \[hep-ph\]](#).
- [43] C. Duhr, A. Vasquez, G. Ventura, and E. Vryonidou, (2025), [arXiv:2503.01954 \[hep-ph\]](#).
- [44] M. Grazzini, A. Ilnicka, M. Spira, and M. Wiesemann, *JHEP* **03**, 115 (2017), [arXiv:1612.00283 \[hep-ph\]](#).
- [45] N. Deuschmann, C. Duhr, F. Maltoni, and E. Vryonidou, *JHEP* **12**, 063 (2017), [Erratum: *JHEP* **02**, 159 (2018)], [arXiv:1708.00460 \[hep-ph\]](#).
- [46] M. Grazzini, A. Ilnicka, and M. Spira, *Eur. Phys. J. C* **78**, 808 (2018), [arXiv:1806.08832 \[hep-ph\]](#).
- [47] J. Hisano, K. Tsumura, and M. J. S. Yang, *Phys. Lett. B* **713**, 473 (2012), [arXiv:1205.2212 \[hep-ph\]](#).
- [48] J. Brod, U. Haisch, and J. Zupan, *JHEP* **11**, 180 (2013), [arXiv:1310.1385 \[hep-ph\]](#).
- [49] V. Cirigliano, W. Dekens, J. de Vries, and E. Mereghetti, *Phys. Rev. D* **94**, 016002 (2016), [arXiv:1603.03049 \[hep-ph\]](#).
- [50] V. Cirigliano, W. Dekens, J. de Vries, and E. Mereghetti, *Phys. Rev. D* **94**, 034031 (2016), [arXiv:1605.04311 \[hep-ph\]](#).
- [51] A. J. Buras and M. Jung, *JHEP* **06**, 067 (2018), [arXiv:1804.05852 \[hep-ph\]](#).
- [52] G. Panico, A. Pomarol, and M. Riembau, *JHEP* **04**, 090 (2019), [arXiv:1810.09413 \[hep-ph\]](#).
- [53] J. Brod and E. Stamou, *JHEP* **07**, 080 (2021), [arXiv:1810.12303 \[hep-ph\]](#).
- [54] M. Bauer, M. Neubert, S. Renner, M. Schnubel, and A. Thamm, *JHEP* **04**, 063 (2021), [arXiv:2012.12272 \[hep-ph\]](#).
- [55] M. Ardu and S. Davidson, *JHEP* **08**, 002 (2021), [arXiv:2103.07212 \[hep-ph\]](#).
- [56] J. Brod, Z. Polonsky, and E. Stamou, *JHEP* **06**, 091 (2024), [arXiv:2306.12478 \[hep-ph\]](#).
- [57] A. Biekötter, J. Fuentes-Martín, A. M. Galda, and M. Neubert, *JHEP* **09**, 120 (2023), [arXiv:2307.10372 \[hep-ph\]](#).
- [58] F. Garosi, D. Marzocca, A. Rodriguez-Sanchez, and A. Stanzione, *JHEP* **12**, 129 (2023), [arXiv:2310.00047 \[hep-ph\]](#).
- [59] L. Allwicher, C. Cornella, G. Isidori, and B. A. Stefanek, *JHEP* **03**, 049 (2024), [arXiv:2311.00020 \[hep-ph\]](#).
- [60] B. A. Stefanek, *JHEP* **09**, 103 (2024), [arXiv:2407.09593 \[hep-ph\]](#).
- [61] J. Fuentes-Martín, P. Ruiz-Femenia, A. Vicente, and J. Virto, *Eur. Phys. J. C* **81**, 167 (2021), [arXiv:2010.16341 \[hep-ph\]](#).
- [62] S. Navas *et al.* (Particle Data Group), *Phys. Rev. D* **110**, 030001 (2024).

- [63] G. Aad *et al.* (ATLAS), *Nature* **607**, 52 (2022), [Erratum: *Nature* **612**, E24 (2022)], [arXiv:2207.00092 \[hep-ex\]](#).
- [64] D. Maitre, *Comput. Phys. Commun.* **174**, 222 (2006), [arXiv:hep-ph/0507152](#).
- [65] T. P. Cheng, E. Eichten, and L.-F. Li, *Phys. Rev. D* **9**, 2259 (1974).
- [66] M. E. Machacek and M. T. Vaughn, *Nucl. Phys. B* **236**, 221 (1984).
- [67] B. Pendleton and G. G. Ross, *Phys. Lett. B* **98**, 291 (1981).
- [68] C. T. Hill, *Phys. Rev. D* **24**, 691 (1981).